

Paper:

# Geometry Optimisation for 2D Cutting: A Quadratic Programming Approach

Florian Sellmann\*, Titus Haas<sup>\*,†</sup>, Hop Nguyen\*, Sascha Weikert<sup>\*\*</sup>,  
and Konrad Wegener\*

\*Institute for Machine Tools and Manufacturing

Tannenstrasse 3, 8092 Zürich, Switzerland

E-mail: info@iwf.mavt.ethz.ch

<sup>\*\*</sup>inspire AG, Technoparkstrasse 1, 8005 Zürich, Switzerland

<sup>†</sup>Corresponding author, E-mail: info@inspire.ethz.ch

[Received July 20, 2015; accepted December 16, 2015]

**A novel approach to geometry optimisation in the field of 2D cutting is presented in this paper. Set point generation inside of state of the art CNCs is divided in the preparation of the geometry and the feed rate generation. The feed rate generation is influenced by parametric derivatives of the given geometry. Due to this fact, the shaping of a B-Spline is carried out by optimisation of the weighted sum of parametric derivatives while the given manufacturing tolerances are maintained. For the sake of robustness, the arising optimisation problem is formulated as a quadratic program with linear constraints, one which can be solved with great efficiency by using an interior point method. In contrast to state of the art methods, the discrete formulation of the problem allows for a pointwise specification of the manufacturing tolerance. Depending on the manufacturing process, the given manufacturing tolerance is shared by different axes, which is shown for a 2D cutting geometry. An application example shows that the geometry optimisation leads to an increase in machining productivity over state of the art methods.**

**Keywords:** geometry optimisation, quadratic programming, optimisation, B-Splines, machine tool

## 1. Introduction

Machining productivity is defined as the number of manufactured parts of a comparable quality per unit of manufacturing time, according to Weck and Brecher [16]. Reducing the processing time while maintaining the required quality therefore increases the productivity of a machine tool.

The set point generation in computerised numerical control (CNC) is divided in two main steps: geometry generation and the feed rate generation, respectively. Due to the fact that the manufacturing of a desired workpiece consists of the relative movement of the tool and the workpiece along spatial trajectories, the surface information of the design has to be converted into NC code using a

computer-aided manufacturing (CAM) tool. For this task, state of the art CAM tools use straight lines and circular arcs, which are discontinuous at the transitions. Discontinuities, high actuator forces, and force rates, respectively, lead to the mechanical excitation of a machine tool, which is a limiting factor of the productivity described above. Therefore, the challenges for geometry optimisation are both the elimination of discontinuities and the reduction of forces and force rates perpendicular to the tool path. For a given feed rate, the resulting deformation of the machine tool is proportional to these forces, which in turn are proportional to the curvature of the tool path.

Optimisation of the tool path is accomplished depending on the NC code, which usually consists of one of the two following programming types.

- Basic geometries, which are described by a sequence of straight lines and circular arcs in order to realise machining operations on the shop floor.
- Freeform curves, which in the majority of cases are described as a sequence of short, straight lines. This type of NC program is usually created by a CAM tool.

Since NC-blocks, such as straight lines and circular arcs, are continuous, the discontinuities are only located at transitions between subsequent NC-blocks, e.g. corners. In this case, state of the art methods in the field of geometry optimisation start and end in the immediate vicinity of the transition. If subsequent NC-blocks have arc lengths of under 1 mm, the smoothing of the transitions is very disadvantageous because the large number of transition points leads to oscillations of the curve, even though if the curvature is continuous. In this case, a global smoothing of multiple NC-blocks is needed. The most challenging task in global smoothing is finding a continuous function that represents the original NC-blocks as smoothly as possible within the given tolerance. In **Fig. 1**, the local and global smoothing of NC-blocks is shown. Based on geometric considerations, several approaches in the field of geometry optimisation have been investigated. For the geometry optimisation and feed rate generation of lin-

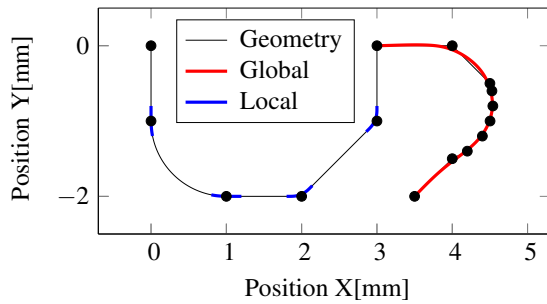


**Fig. 1.** Planar geometry consisting of circular arcs and straight lines. The global smoothing of multiple NC-blocks is denoted by the red line. The rounding of the transitions of subsequent NC-blocks, i.e. local smoothing, is denoted by blue lines.

ear systems, Yu [17] presents algorithms which are based on the spline representation of the tool path and which use spline-based interpolation and approximation methods. Morishige and Kaneko [10] use B-Splines to obtain continuous movements of the machine tool and less movement of the rotational axes, therefore, producing an excellent finished surface for milling with a ball end mill. Bouard et al. [4] minimise the curvature of the regarded trajectory while ensuring the constraints given by the process and geometry. Hadorn [8] also minimises the curvature of an assumed smoothing spline. In his work, methods for both the smoothing of the transition between subsequent NC-blocks with quintic Bezier-Splines and the global smoothing of multiple NC-blocks with cubic beta-Splines are investigated. For the continuous connection between a quintic Bezier-Spline and the given geometry, the  $\lambda$ -parametrisation is investigated. It is generalised for a B-Spline of degree  $p$  in section 3.3. Regarding the global smoothing of multiple NC-blocks with beta-splines, the convex hull property of these types of curves is used for the shaping, since the control points of the smoothing spline are chosen in such a way that the resulting curve remains within the convex hull of the polygon given by the control points. Zhao et al. [18] show the analytic smoothing of multiple G01 blocks with B-Splines. In addition, feed rate constraints are evaluated along the tool-path. Established in the field of CAD, Park and Lee [12] evaluate dominant points of a given discrete curve in response to the curvature. Therefore, only discrete points at curve sections with large curvatures are considered for a subsequent approximation. In the case of discontinuities or high curvatures of the discretised geometry, this approach leads to an unintended accumulation of control points and a bad shape of the approximated curve, as well as to a low feed rate.

In order to decrease machining time, Boz et al. [5] investigate a feed scheduling strategy for the calculation of the desired feed rate with respect to the maximum allowable cutting force. Feed rate scheduling leads to shorter cycle times than when the feed rate is constant. Although this method produces higher local feed rates and shorter machining times, the continuity of the trajectory is not increased.

Taking into account that the resulting feed rate is directly affected by the parametric derivatives of a given geometry, Beudaert et al. [3] show an approach to the smoothing of 5-axis tool paths in order to maximise the resulting feed rate via the local smoothing of single axes. A quadratic programming (QP) approach with linear constraints for the smoothing spline is implemented by Kano et al. [9]. Although the deviation between the smoothing function and the programmed trajectory is limited during optimisation, there is no tolerance sharing between the axes involved in the optimisation. Consequently, a full exploitation of the manufacturing tolerance is not achieved with this approach. Another QP approach in the field of geometry optimisation is given by Haas [7]. In this work, in order to limit the resulting deviation perpendicular to the tool path, higher parametric derivatives of the smoothing curve are minimised with respect to linear constraints on the tool path in the case of 2D cutting. The decrease in machine excitation is evaluated using a 2-mass-spring model and measurements on a real machine.

As mentioned above, the subsequent calculated feed rate is affected by the parametric derivatives of the geometry. Due to this fact, there is a need for a global optimisation of these derivatives while exploiting the given manufacturing tolerances in order to increase productivity. State of the art algorithms in the field of geometry optimisation deal with a global limitation of the manufacturing tolerance, which is identified regarding the worst case of the machine tool within the work space. In contrast, a point-wise limitation of the path deviation would allow for a better exploitation of the given manufacturing tolerances.

The paper is organised as follows. General remarks, including fundamentals of curves and path dynamics, are given in section 2. A method for discrete geometry optimisation (DGO), including the cost function as well as the constraints and boundaries for the optimisation, is presented in section 3. In section 4, both a machine model and a virtual CNC for the simulation of the feed rate generation are presented. Examples of the method are given in section 5. Section 6 presents the conclusions of this paper.

## 2. General Remarks

For geometry optimisation, parametric curves with respect to an increasing parameter  $s$  are used. The movement of the tool center point (TCP) is denoted as  $\underline{r}(s)$  and describes the relative movement of the tool and the workpiece in a workpiece fixed coordinate system. While vector quantities have a single underline, matrix quantities have a double underline. Thus  $\underline{x}_i$  denotes the  $i$ -th element of a vector  $\underline{x}$ .

### 2.1. Properties of Curves

The following definitions are based on Aminov [1] and are valid for the curves in the remainder of this paper. A  $d$ -dimensional parametric curve is defined as follows.

**Definition 2.1:** A parametric curve in  $\mathbb{R}^d$  is the map  $r : I \rightarrow \mathbb{R}^d$  of the closed interval  $I := [l_b, u_b]$  to  $\mathbb{R}^d$ .

Important parameters in the remainder of this paper are the parametric derivatives  $\underline{r}^{(i)}(s)$ , which are defined as follows.

**Definition 2.2:** The  $i$ -th parametric derivative of  $\underline{r}(s)$  is defined as  $\underline{r}^{(i)}(s) = \frac{d^i}{ds^i} \underline{r}(s)$ .  $\underline{r}'(s)$  is the first parametric derivative and is called the parametric velocity,  $\underline{r}''(s)$  is the second parametric derivative and is called the parametric acceleration.

The regularity of curves is defined as follows.

**Definition 2.3:**  $\underline{r}'(s) \neq 0 \forall s \in I := [l_b, u_b]$

Since feed rate generation will be unfeasible if  $\underline{r}'(s) = 0$  nonregular curves are not considered. Regarding the continuity of curves, parametric continuity must be distinguished from geometric continuity. Parametric continuity is defined as follows.

**Definition 2.4:** A curve  $\underline{r}(s)$  is said to be  $C^n$  continuous if the  $n$ -th derivative  $\frac{d^n \underline{r}}{ds^n}$  is continuous for  $s \in [l_b, u_b]$ .

The geometric continuity in the following, denoted, according to Bartels et al. [2], as  $G^n$  continuity of a curve with the parameter  $n$  as a measurement of the smoothness, is defined as follows.

**Definition 2.5:** Assuming a parametric curve  $\underline{r}(s)$  of the  $\mathbb{R}^3$  in the closed interval  $s \in [l_b, u_b]$  the first three orders of geometric continuity are described as follows.

- $G^0$ : The curve is continuous.
- $G^1$ : The direction but not necessarily the magnitude of the tangent vector is continuous. In other words, this is a curve without any corners.
- $G^2$ : The direction but not necessarily the magnitude of the curvature vector is continuous.

Discontinuous forces and high force rates lead to mechanical excitation of the machine tool, which reduces productivity according to Steinlin [15]. For this reason, the curve has to be at least  $G^2$  continuous. Using the Frenet formulae, the parametric derivatives of a curve in  $\mathbb{R}^3$  lead to the Frenet frame  $\underline{\theta}(s) = \{\underline{e}_t(s), \underline{e}_n(s), \underline{e}_b(s)\}$ , which is defined as follows.

$$\underline{e}_t(s) = \frac{\underline{r}'(s)}{|\underline{r}'(s)|} \quad \dots \quad (1)$$

$$\underline{e}_n(s) = \frac{(\underline{r}'(s) \times \underline{r}''(s)) \times \underline{r}'(s)}{|(\underline{r}'(s) \times \underline{r}''(s)) \times \underline{r}'(s)|} \quad \dots \quad (2)$$

$$\underline{e}_b(s) = \underline{e}_t(s) \times \underline{e}_n(s) \quad \dots \quad (3)$$

The Frenet frame of a curve is shown in **Fig. 2**.  $\underline{e}_t(s)$  and  $\underline{e}_n(s)$  span the osculating plane. The curvature circle lies in this plane, as shown in **Fig. 2**. While  $\underline{e}_t(s)$  is tangential to the curvature circle,  $\underline{e}_n(s)$  is perpendicular to it and denotes the direction of a connecting line between the point on the curve and the center of the curvature circle.

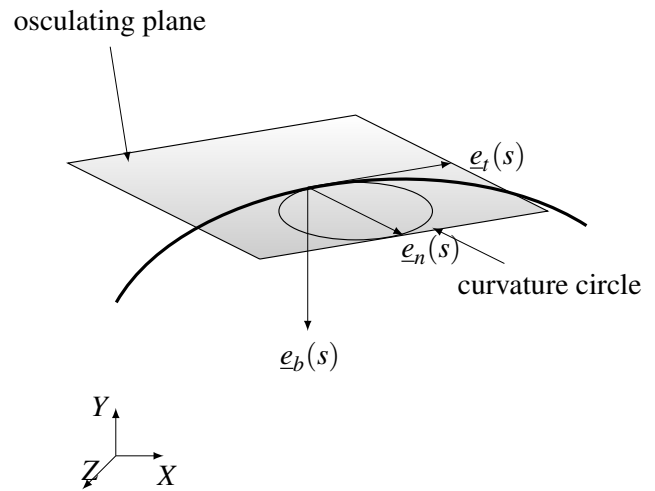


**Fig. 2.** Frenet frame, osculating plane and curvature circle of a parametric curve.

The reciprocal value of the radius of the curvature circle is called the curvature  $\kappa$ .

$$\kappa = \frac{|\underline{r}' \times \underline{r}''|}{|\underline{r}'|^3} \quad \dots \quad (4)$$

It describes the rate of change of the direction of  $\underline{e}_t(s)$  along the arc length of the curve.

## 2.2. B-Splines

For the geometry description, different types of continuous curves are available on state of the art open-loop controllers. Unlike polynomial functions, B-Splines are not prone to undesirable oscillations and are, therefore, used for the description of the optimised geometries. The following explanations are based on Piegl and Tiller [13].

The Basis-Spline in the following, denoted as B-Spline of degree  $p$ , is defined as the linear combination of the control points  $\underline{a}_i$  with the  $i$ th B-Spline basis function  $N_{i,p}(s)$  of the degree  $p$ :

$$\underline{r}(s) = \sum_{i=0}^m N_{i,p}(s) \underline{a}_i \quad l_b \leq s \leq u_b \quad \dots \quad (5)$$

The recursively defined  $i$ th B-Spline basis functions of degree  $p$  is obtained for  $p > 1$  as

$$N_{i,p}(s) = \frac{s - s_i}{s_{i+p} - s_i} N_{i,p-1}(s) + \frac{s_{i+p+1} - s}{s_{i+p+1} - s_{i+1}} N_{i+1,p-1}(s) \quad \dots \quad (6)$$

with

$$N_{i,0}(s) = \begin{cases} 1 & \text{if } s_i \leq s \leq s_{i+1} \\ 0 & \text{otherwise} \end{cases} \quad \dots \quad (7)$$

$s_i$  are knots. At every knot, the description of the basis function changes. All  $s_i$  lead to the knot sequence  $\underline{u}$  of the length  $m + p + 1$ . For the evaluation of the knot sequence, closed, open, or clamped curves must be distinguished between. In the following, only clamped curves, which in-

terpolate the first and last control points, are regarded. For these types of curves, the knot sequence is defined as

$$\underline{u} = [ \underbrace{l_b, \dots, l_b}_{p+1}, \dots, u_{m-p-1}, \underbrace{u_b, \dots, u_b}_{p+1} ] . . . . (8)$$

Characteristic is the  $p + 1$ -fold occupation of the first and last node and the aperiodic internal nodes.

### 3. Discrete Geometry Optimisation

While all given quantities are denoted with an upper bar in the following, the optimised quantities are denoted with a tilde.

Assuming a given tool path  $\bar{r}(s)$ , which consists of the NC-blocks  $\bar{r}^1(s)$  to  $\bar{r}^h(s)$  with  $0 \leq s \leq 1$ , an at least  $G^2$  continuous curve  $\tilde{r}(s)$  with a minimum curvature at every point along the tool path is sought. This leads to an optimisation problem including a cost function, constraints, and boundaries. In favor of robustness, the problem is formulated as a quadratic program (QP) in order to find a vector  $\underline{x}$ , which minimises the scalar cost function

$$J = \frac{1}{2} \underline{x}^T \underline{H} \underline{x} + \underline{c}^T \underline{x} . . . . . (9)$$

subject to the linear equality constraints

$$\underline{A}_{eq} \underline{x} = \underline{b}_{eq} . . . . . (10)$$

and the linear inequality constraints

$$\underline{A} \underline{x} \leq \underline{b} . . . . . (11)$$

$\underline{H}$  denotes a symmetric matrix and represents the quadratic part of (9). The vector  $\underline{c}$  represents the linear part of (9).

#### 3.1. Cost Function

By minimising the parametric derivatives  $\tilde{r}^{(k)}(s)$  of the smoothing function, the cost function is defined as

$$J = \sum_{i=1}^p \int_{s_a}^{s_b} \eta_i (\tilde{r}^{(i)}(s))^2 ds . . . . . (12)$$

with  $p$  the number of considered parametric derivatives,  $\eta_i$  the weights (which are further explained in section 3.4),  $s_a$  the start, and  $s_b$  the end parameter.

The cost function (12) has to be reformulated in the form of (9). The resulting QP problem has to be convex; the matrix  $\underline{H}$  in (9) must be positive semidefinite, assuming a feasible solution. The smoothing function  $\tilde{r}(s)$  is represented by B-Splines of degree  $p$ . These are given by a knot sequence  $\underline{u}$  for the evaluation of the B-Spline basis functions  $N_{i,p}(s)$  and the control points  $\underline{a}_i$ , which influence the shape of the curve. The vector  $\underline{x}$  in (9) consists of the coordinates of the  $m$  control points, which optimise the curve according to the cost function  $J$ . Assuming a knot sequence  $\underline{u}$  with  $m + p + 1$  entities and a parameter

vector  $\hat{s}$  with  $n$  values leads to

$$\tilde{r}^{(k)}(\hat{s}) = \sum_{i=0}^m N_{i,p}^{(k)}(\hat{s}) a_i = \underline{C}^{(k)}(\hat{s}) \underline{a} . . . . . (13)$$

with  $\underline{C}^{(k)}(s)$  including the basis functions  $N_{i,p}^{(k)}(s)$  evaluated at the parameter values  $\hat{s}$ . In order to realise a good shape of  $\tilde{r}^{(k)}(s)$ , both a parameter vector  $\hat{s}$  and an appropriate knot sequence  $\underline{u}$  must be selected. Three methods for the parameterisation, assuming that the parameter  $s$  lies in the range  $s \in [0, 1]$ , are described by Piegl and Tiller [13]. In the following DGO algorithm, the parametrisation proportional to the chord length is used. The chord length  $L$  is defined by

$$L = \sum_{i=0}^{n-1} |r_{i+1} - r_i| . . . . . (14)$$

Then the parameter values are given as

$$s_i = s_{i-1} + \frac{|r_i - r_{i-1}|}{L} \quad i = 1, \dots, n . . . . . (15)$$

with

$$s_0 = 0 . . . . . (16)$$

For the parametrisation, a suitable knot sequence has to be defined. The following technique of averaging for the computation of  $\underline{u} = \{u_0, \dots, u_m\}$  is recommended by Piegl and Tiller [13, 14]. It is

$$u_0 = \dots = u_p = 0 . . . . . (17)$$

$$u_{m-p} = \dots = u_m = 1 . . . . . (18)$$

and

$$u_{j+p} = \frac{1}{p} \sum_{i=j}^{j+p-1} s_i \quad j = 1, \dots, n-p . . . . . (19)$$

With this method, the knot sequence  $u$  reflects the distribution of the parameter values  $\hat{s}$  and supports a good shape for the resulting curve. Inserting (13) in (12) with the given parametrisation  $\hat{s}$  and the  $j$ th increment  $\Delta s_j$  leads to

$$\begin{aligned} J &= \sum_{k=1}^p \int_{s_a}^{s_b} \eta_k (\tilde{r}^{(k)}(s))^2 ds \\ &= \sum_{k=1}^p \sum_{i=1}^n \eta_k (\tilde{r}^{(k)}(\hat{s}_i))^2 \\ &= \sum_{k=1}^p \sum_{i=1}^n \eta_k (\underline{C}^{(k)}(\hat{s}_i) \underline{a})^2 . . . . . (20) \end{aligned}$$

Therefore,  $\underline{H}$  and  $\underline{c}$  in (9) are defined by

$$\underline{H} = \sum_{k=1}^p \eta_k \underline{C}^{(k)T} \underline{C}^{(k)} . . . . . (21)$$

$$\underline{c} = \underline{0} . . . . . (22)$$

The matrix  $\underline{H}$  is positive semidefinite due to the fact that the matrix represents a squared linear combination of parametric derivatives. Therefore, (12) is convex, as-





degree  $p$  in the following.

A B-Spline curve shall be computed in order to connect the two given points  $\underline{r}_a$  and  $\underline{r}_b$ . In the remainder of this section,  $a$  and  $b$  refer to the beginning and the end of the curve, respectively. The local Frenet frames at the beginning and the end of the curve are given as  $\underline{\theta}_a$  and  $\underline{\theta}_b$ , respectively. Boundary conditions for the curvature are given by  $\kappa_a$  at  $s = 0$  and  $\kappa_b$  at  $s = 1$ . If there are linear axes and  $\tilde{\underline{r}}(s)$  is connected with common NC-blocks like straight lines and circular arcs, the following demands on the parametric derivatives at the start

$$\underline{r}_a = \tilde{\underline{r}}(s=0) \quad . \quad . \quad . \quad . \quad . \quad . \quad (35)$$

$$\lambda_a \underline{e}_{t,a} = \tilde{\underline{r}}'(s=0) \quad . \quad . \quad . \quad . \quad . \quad . \quad (36)$$

$$\kappa_a = \frac{|\tilde{\underline{r}}'(s=0) \times \tilde{\underline{r}}''(s=0)|}{|\tilde{\underline{r}}'(s=0)|^3} \quad . \quad . \quad . \quad . \quad . \quad . \quad (37)$$

$$0 = \tilde{\underline{r}}'(s=0) \cdot \tilde{\underline{r}}''(s=0) \quad . \quad . \quad . \quad . \quad . \quad . \quad (38)$$

and the end of the curve

$$\underline{r}_b = \tilde{\underline{r}}(s=1) \quad . \quad . \quad . \quad . \quad . \quad . \quad (39)$$

$$\lambda_b \underline{e}_{t,e} = \tilde{\underline{r}}'(s=1) \quad . \quad . \quad . \quad . \quad . \quad . \quad (40)$$

$$\kappa_b = \frac{|\tilde{\underline{r}}'(s=1) \times \tilde{\underline{r}}''(s=1)|}{|\tilde{\underline{r}}'(s=1)|^3} \quad . \quad . \quad . \quad . \quad . \quad . \quad (41)$$

$$0 = \tilde{\underline{r}}'(s=1) \cdot \tilde{\underline{r}}''(s=1) \quad . \quad . \quad . \quad . \quad . \quad . \quad (42)$$

occur in order to fulfill the given boundary conditions described above.

Since only clamped curves defined by the knot sequence (8) are used in this work,  $\tilde{\underline{r}}(s)$  interpolates the first and the last control point, so  $G^0$  and  $C^0$  continuity are ensured by  $\underline{a}_0 = \underline{r}_a$  and  $\underline{a}_n = \underline{r}_b$ .

According to Piegel and Tiller [14], the first two parametric derivatives of a B-Spline of degree  $p$  for  $s = 0$  and  $s = 1$  are defined as

$$\underline{r}'(s=0) = \frac{p}{u_{p+1}}(\underline{a}_1 - \underline{a}_0) \quad . \quad . \quad . \quad . \quad . \quad . \quad (43)$$

$$\underline{r}'(s=1) = \frac{p}{1 - u_{m-p-1}}(\underline{a}_n - \underline{a}_{n-1}) \quad . \quad . \quad . \quad . \quad . \quad . \quad (44)$$

$$\underline{r}''(s=0) = \frac{p(p-1)}{u_{p+1}} \left( \frac{\underline{a}_0}{u_{p+1}} - \frac{(u_{p+1} + u_{p+2})\underline{a}_1}{u_{p+1}u_{p+2}} + \frac{\underline{a}_2}{u_{p+2}} \right) \quad (45)$$

$$\underline{r}''(s=1) = \frac{p(p-1)}{1 - u_{m-p-1}} \left( \frac{\underline{a}_n}{1 - u_{m-p-1}} + \frac{\underline{a}_{n-2}}{1 - u_{m-p-2}} - \frac{(2 - u_{m-p-1} - u_{m-p-2})\underline{a}_{n-1}}{(1 - u_{m-p-1})(1 - u_{m-p-2})} \right) \quad (46)$$

As already defined by Hadorn [8], the 6  $\lambda$ -parameters  $\lambda_0 \dots \lambda_5$  are introduced in order to ensure a  $G^2$ -continuous movement of the control points at the start and the end of  $\tilde{\underline{r}}(s)$  on the osculating plane spanned by the local Frenet

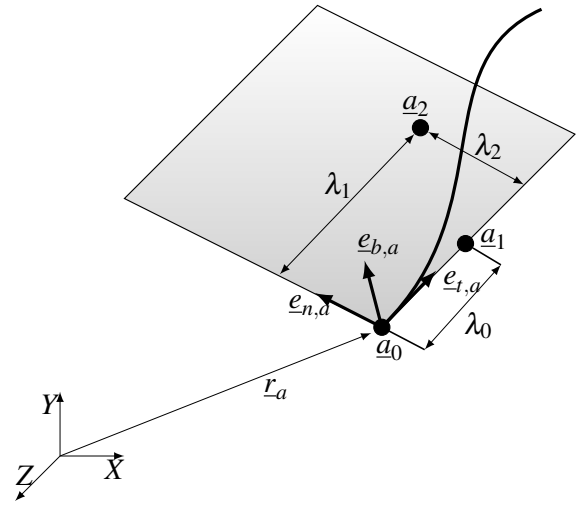


**Fig. 4.**  $\lambda$ -parametrisation for the begin of a B-Spline. As defined in (47) and (48) by modification of  $\lambda_0 \dots \lambda_2$  the control points  $\underline{a}_1$  and  $\underline{a}_2$  are moved on the osculating plane spanned by the local Frenet frame  $\underline{\theta}_a$ .

frames  $\underline{\theta}_a$  and  $\underline{\theta}_b$ , which is evaluated at the transitions between  $\tilde{\underline{r}}(s)$  and  $\tilde{\underline{r}}(s)$ . According to **Fig. 4**, the control points at the start and the end of  $\tilde{\underline{r}}(s)$  are defined as

$$\underline{a}_1 = \underline{a}_0 + \lambda_0 \underline{e}_{t,a} \quad . \quad . \quad . \quad . \quad . \quad . \quad (47)$$

$$\underline{a}_2 = \underline{a}_0 + \lambda_1 \underline{e}_{t,a} + \lambda_2 \underline{e}_{n,a} \quad . \quad . \quad . \quad . \quad . \quad . \quad (48)$$

$$\underline{a}_{n-1} = \underline{a}_n - \lambda_5 \underline{e}_{t,e} \quad . \quad . \quad . \quad . \quad . \quad . \quad (49)$$

$$\underline{a}_{n-2} = \underline{a}_n - \lambda_4 \underline{e}_{t,e} + \lambda_3 \underline{e}_{n,e} \quad . \quad . \quad . \quad . \quad . \quad . \quad (50)$$

Insertion of (47)-(50) in (43)-(46) leads to

$$\lambda_1 = \lambda_0 \frac{u_{p+1} + u_{p+2}}{u_{p+1}} \quad . \quad . \quad . \quad . \quad . \quad . \quad (51)$$

$$\lambda_2 = \frac{\kappa_a u_{p+2} \lambda_0^2 p}{u_{p+1}(p-1)} \quad . \quad . \quad . \quad . \quad . \quad . \quad (52)$$

$$\lambda_4 = \lambda_5 \frac{u_{m-p-1} + u_{m-p-2} - 2}{u_{m-p-1} - 1} \quad . \quad . \quad . \quad . \quad . \quad . \quad (53)$$

$$\lambda_3 = \frac{\kappa_b (u_{m-p-2} - 1) \lambda_5^2 p}{(u_{m-p-1} - 1)(p-1)} \quad . \quad . \quad . \quad . \quad . \quad . \quad (54)$$

for the fulfillment of (35) -(42). Obviously  $\lambda_0$  and  $\lambda_5$  are free parameters for the shaping of the curve while ensuring the continuity conditions at the boundaries described above. The  $\lambda$ -parameterisation is part of the optimisation since (51)-(54) can be established as additional linear constraints.

### 3.4. Parametrisation

While the optimisation problem with respect to the given constraints and boundaries is formulated, some parameters are still free. These are the number  $m$  of control points, which are used for the optimisation, the degree  $p$  of the B-Spline, and the additional weights  $\eta_k$  in the cost function (12). In order to retain the convexity of the underlying optimisation problem, these parameters

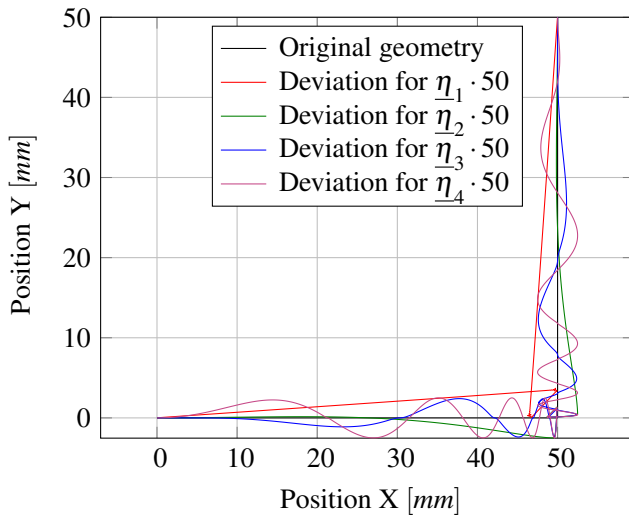


**Fig. 5.** Deviation in normal direction of the tool path in response to the tuple of the used weighting factors  $\eta$ .

are varied iteratively and evaluated on different geometries in order to identify a parameter set with maximum productivity.

The shape of the resulting B-Spline is influenced by the number of control points. The fewer the points, the more global the behavior of the optimised curve.

In (12), the different parametric derivatives of  $\underline{r}(s)$  are weighted by  $\eta_k$ . The effect of the parameter weighting for a quintic B-Spline is exemplified on a planar rectangular corner with a permissible deviation of  $50 \mu\text{m}$  in the normal direction, as can be seen in **Fig. 5**. The following tuples  $\underline{\eta}_i$  are used for the optimisation.

- $\underline{\eta}_1 = \{1, 0, 0, 0\}$ : Minimum of the parametric speed
- $\underline{\eta}_2 = \{0, 1, 0, 0\}$ : Minimum of the parametric acc.
- $\underline{\eta}_3 = \{0, 0, 1, 0\}$ : Minimum of the parametric jerk
- $\underline{\eta}_4 = \{0, 0, 0, 1\}$ : Minimum of the parametric jerk-rate

As can be seen in **Fig. 5**, the weighting of the parametric jerk  $\underline{\eta}_3$  and of the parametric jerk-rate  $\underline{\eta}_4$  leads to unintended oscillations in the shape of the B-Spline. This is caused by the different order of magnitude of the different parametric derivatives, so small changes in function values of the higher derivatives lead to large changes in the function values of the lower derivatives. Thus, only a minimisation of the parametric speed and acceleration will result in a curve  $\tilde{\underline{r}}(s)$  of adequate shape. Knowing that the arc length of a spatial curve is influenced by the parametric speed  $\underline{r}'(s)$ , a minimisation with  $\underline{\eta}_1$  leads to a minimisation of the arc length and a high local curvature. An adequate shape is obtained using  $\underline{\eta}_2$ , which is proportional to the parametric acceleration and the curvature, respectively. According to Beudaert et al. [3], a minimisation of the second parametric derivative, which is proportional to the curvature (4), leads to a smooth trajectory. This leads to  $\eta = \{0, 1, 0, 0\}$ .

**Table 1.** Maximum Velocity and maximum acceleration of the simulated machine tool.

	Max. Velocity	Max. Acceleration
X-axis	100 m/min	0.9 g
Y-axis	100 m/min	1 g

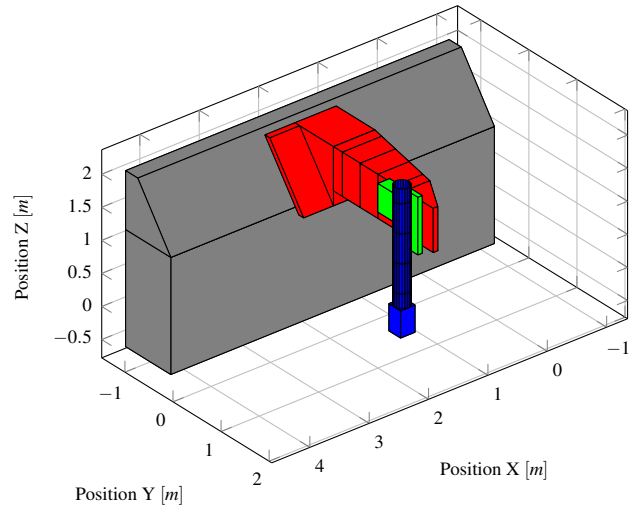


**Fig. 6.** Machine model of the 5-axis cutting machine tool.

## 4. Simulation

In the following, the simulation environment including a machine model and a virtual CNC are presented.

### 4.1. Virtual CNC

Since this paper is about geometry optimisation, the feed rate for the illustration of the effects of the DGO is obtained using a virtual CNC. The virtual CNC is commercial software, presented by Bretschneider and Menzel [6], for the purpose of validating given NC-Code. It consists of an image of a Siemens 840D open loop controller of a 5-axis machine tool with the feed rate constraints for the X- and Y-axis listed in **Table 1**. The output of the virtual CNC is a time-discrete representation of the feed rate along the tool path, which is specified in the NC-Code. A limitation of the Z-axis is not necessary because the example is 2-dimensional.

For the evaluation of a time-discrete profile of the feed rate, the optimised geometry  $\tilde{\underline{r}}(s)$ , available as a B-Spline, is converted into NC-Code and given to the open loop controller. The execution of the resulting NC-Code leads to the required time-discrete profile of the feed rate, which is given to a machine model for the simulation of the contouring error.

### 4.2. Machine Model

**Figure 6** shows a machine model, based on Nguyen et al. [11] and explained in the following. It is a rigid-body model including a model for the control system.

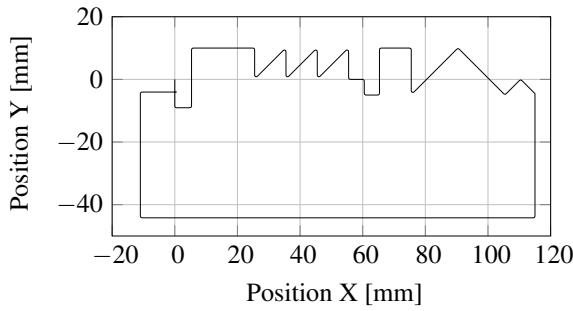


**Fig. 7.** 2D geometry which is optimised with the DGO using the parameters which are identified in 3.4. The clockwise motion starts in (0,0).

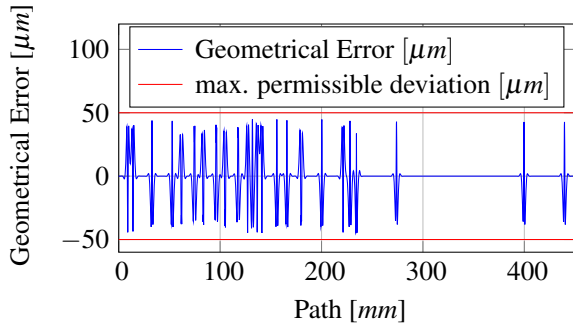


**Fig. 8.** Programmed deviation in orthogonal direction between  $\tilde{\mathbf{r}}(s)$  and  $\tilde{\mathbf{r}}(s)$  along the tool path.

In the low to medium frequency range in machine tools, motion primarily takes place in the coupling locations between the mechanical machine components, such as the linear guideways or rotary bearings. Therefore, the deformation behavior in the low to medium frequency range is actually given by the deflection of these coupling elements. This allows for an approach with multi body dynamics, which finally leads to results comparable to those obtained by Finite Element Methods.

The model structure shown in **Fig. 6** is coupled with a control system. The machine tool can therefore be simulated with regard to its structural behavior as well as its control parameters even in an early phase of the machine tool design. In this context, the model explained above is used for the simulation of the system response of an existing machine tool.

## 5. Application Example

To illustrate the effects of the DGO on machine oscillations and the resulting feed rate, the planar geometry shown in **Fig. 7** is rounded with a global tolerance value in the normal direction of the tool path of 50  $\mu\text{m}$ . The exploitation of the given tolerance in the normal direction is shown in **Fig. 8**. Using the parametrisation described above leads to  $\tilde{\mathbf{r}}(s)$ , which is inserted into the virtual CNC in order to obtain a time-discrete feed rate profile. This is applied to the described machine model.

Regarding the resulting feed rate profile for the refer-

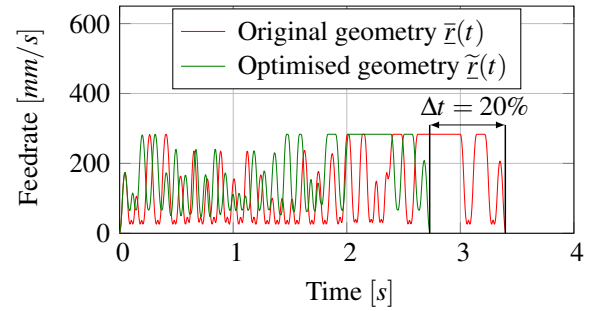


**Fig. 9.** Feed rate profiles, generated by the virtual CNC for the original geometry (red) and the optimised geometry (green). Due to the decreased speed drops of the optimised geometry, a time saving of 20% is achieved.

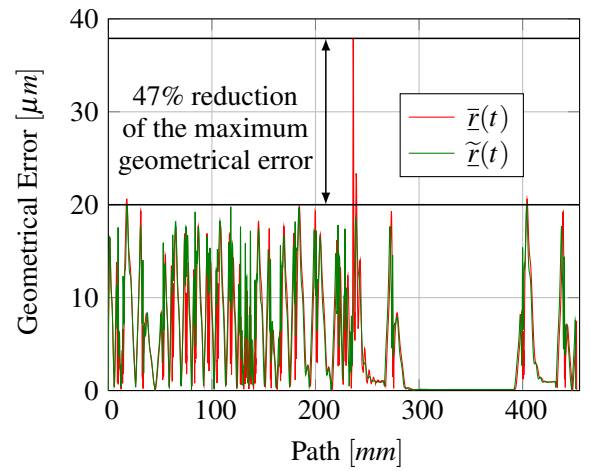


**Fig. 10.** Spatial deviation between the TCP and the linear encoders of the machine tool axes.

ence geometry  $\tilde{\mathbf{r}}(s)$ , shown in **Fig. 9**, speed drops at the transitions between the different NC-blocks occur. The geometry  $\tilde{\mathbf{r}}(s)$  carried out by the DGO is  $G^2$  continuous, therefore, providing a better feed rate since speed drops at transitions are significantly reduced. This leads to a time savings of 20%.

In order to evaluate the mechanical excitation of the machine tool, the machine model described in section 4 is used. The resulting modeled deviation  $\Delta_n$  at the TCP consists of systematic errors  $\Delta_{smt}$  caused by the smoothing of  $\tilde{\mathbf{r}}(s)$ , follow-up errors  $\Delta_{fup}$  generated inside of the closed loop controller, and dynamic errors  $\Delta_{dyn}$  with respect to (55).

$$\Delta_n = \Delta_{smt} + \Delta_{fup} + \Delta_{dyn} \quad \dots \quad (55)$$

The dynamic errors  $\Delta_{dyn}$  as well as the follow-up errors  $\Delta_{fup}$  are separated by the evaluation of the spatial difference between the linear encoders of the machine tool axes and the TCP. As can be seen in **Fig. 10**, the maximum spatial deviation between the TCP and the linear encoders of the machine tool axes (and therefore the mechanical excitation) can be reduced slightly through optimisation.



## 6. Conclusion

The presented DGO minimises the weighted sum of the parametric derivatives of different axes while ensuring the geometric constraints and boundaries, which are given by the manufacturing tolerances. The optimised geometry is described by B-Splines. As the problem formulation for the optimisation is convex, the optimisation succeeds for all given optimisation cases, assuming there is a feasible solution. With this method, both the rounding of transitions of adjoining NC-blocks and the global smoothing of multiple short NC-blocks are accomplished. On the basis of an application example, it is shown that the presented method not only decreases machine excitations but also increases the feed rate, thus increasing productivity. Geometry optimisation alone does not usually generate time-optimal curves. For this, further studies should focus on subsequent and combined optimisation of set point generation.

## References:

- [1] Y. Aminov, "Differential Geometry and Topology of Curves," CRC Press, 2000.
- [2] R. Bartels, J. Beatty, and B. A. Barsky, "An introduction to Splines for use in Computer Graphics & Geometric Modeling," Morgan Kaufmann Publishers, Inc, Los Altos, California 94022, 1987.
- [3] X. Beudaert, P.-Y. Pechard, and C. Tournier, "5-Axis tool path smoothing based on drive constraints," International Journal of Machine Tools and Manufacture, Vol.51, No.12, pp. 958–965, 2011.
- [4] M. Bouard, V. Pateloup, and P. Armand, "Pocketing toolpath computation using an optimization method," Computer-Aided Design, Vol.43, No.9, pp. 1099–1109, 2011.
- [5] Y. Boz, O. Demir, and I. Lazoglu, "Model Based Feedrate Scheduling for Free-Form Surface Machining," International Journal of Automation Technology, Vol.4, pp. 273–283, 2010.
- [6] J. Bretschneider and T. Menzel, "Virtual Optimization of Machine Tools and Production Processes," International Journal of Automation Technology, Vol.1, pp. 136–140, 2007.
- [7] T. Haas, "Diskrete Geometrieoptimierung und Interpolationsmethoden für die Laserschneidbearbeitung," Master's thesis, ETH Zürich, Switzerland, 2012.
- [8] M. Hadorn, "Optimal Set Point Generation for Machine Tools under Nonlinear Constraints," PhD thesis, ETH Zürich, Switzerland, 2007. DISS. ETH Nr. 1132.
- [9] H. Kano, H. Fujioka, and C. F. Martin, "Optimal smoothing and interpolating splines with constraints," Applied Mathematics and Computation, Vol.218, No.5, pp. 1831–1844, 2011.
- [10] K. Morishige and M. Kaneko, "Tool Path Generation for Five-Axis Controlled Machining with Consideration of Motion of Two Rotational Axes," International Journal of Automation Technology, Vol.5, pp. 412–419, 2011.
- [11] M. H. Nguyen, S. Weikert, and K. Wegener, "Toolbox for control system analysis of machine tools," In Proceedings of the 13<sup>th</sup> Mechatronic Forum International Conference, Linz, Austria, 2012.
- [12] H. Park and J.-H. Lee, "B-spline curve fitting based on adaptive curve refinement using dominant points," Computer-Aided Design, Vol.39, No.6, pp. 439–451, 2007.
- [13] L. Piegl and W. Tiller, "The NURBS Book," Springer, 1996.
- [14] L. Piegl and W. Tiller, "Least-Squares B-Spline Curve Approximation with Arbitrary End Derivatives," Engineering with Computers, Vol.16, pp. 109–116, 2000.
- [15] M. Steinlin, "Model based Feed-rate Optimization for Machine Tool Trajectories," PhD thesis, ETH Zürich, Switzerland, 2012.
- [16] M. Weck and C. Brecher, "Werkzeugmaschinen," Springer Berlin, Heidelberg, New York, 2005.
- [17] G. Yu, "Optimale Steuerung der Bewegung und der Geschwindigkeit für das drei- und fünfachsiges Fräsen," PhD thesis, ETH Zürich, Switzerland, 1996.
- [18] H. Zhao, L. Zhu, and H. Ding, "A real-time look-ahead interpolation methodology with curvature-continuous B-spline transition scheme for CNC machining of short line segments," International Journal of Machine Tools and Manufacture, Vol.65, No.0, pp. 88–98, 2013.



### Name:

Florian Sellmann

### Affiliation:

Ph.D. Student, Institute for Machine Tools and Manufacturing (IWF), ETH Zürich

### Address:

Tannenstrasse 3, 8092 Zürich, Switzerland

### Brief Biographical History:

2007 Dipl. Ing., Mechanical Engineering, TU Darmstadt  
2008- Research Assistant and Doctoral Student, Institute of Machine Tools and Manufacturing IWF, ETH Zürich

### Main Works:

- "Model based calculation of the tool-path smoothing tolerances," 27th Annual Meeting of the ASPE, San Diego/USA, 2012.
- "Improvement of the dynamic behavior of machine tools by geometrical optimization of the machine tool axes movements," Proc. of the 13th Mechatronic Conf., Linz, Austria, 2012.



### Name:

Titus Haas

### Affiliation:

Ph.D. Student, inspire AG

### Address:

Technoparkstrasse 1, 8005 Zürich, Switzerland

### Brief Biographical History:

2013 Graduated Masters of Mechanical Engineering, ETH Zürich  
2013- Research Assistant and Doctoral Student, inspire AG



### Name:

Hop Nguyen

### Affiliation:

Ph.D. Student, Institute for Machine Tools and Manufacturing (IWF), ETH Zürich

### Address:

Tannenstrasse 3, 8092 Zürich, Switzerland

### Brief Biographical History:

2009 Graduated Masters of Mechanical Engineering ETH Zürich  
2009- Research Assistant and Doctoral Student, Institute of Machine Tools and Manufacturing IWF, ETH Zürich

### Main Works:

- "Toolbox for control system analysis of machine tools," Proc. of the 13th Mechatronic Conf., Linz, Austria, 2012.
- "Evaluation method for direct evaluations of acceleration correlated position errors in machine tools," 27th Annual Meeting of the ASPE, San Diego/USA, 2012.
- "Measurement and simulation of acceleration correlated position errors in machine tools," LAMDAMAP 2013, Bedfordshire, England, 2013.



**Name:**  
Sascha Weikert

**Affiliation:**  
Group Leader Simulation, Institute for Machine  
Tools and Manufacturing (IWF), ETH Zürich

**Address:**  
Technoparkstrasse 1, 8005 Zürich, Switzerland

**Brief Biographical History:**

2000 Ph.D., ETH Zürich  
2000- Institute for Machine Tools and Manufacturing (IWF), ETH Zürich  
2015- inspire AG

**Main Works:**

- “Thermal behaviour improvement of linear axis,” Proc. of the 11th euspen Conf., Como, Italy, 2011.
- “Evaluation of modelling approaches for machine tool design,” Precision Engineering, Vol.34, pp. 399-407, 2010.
- “R-Test, a new device for accuracy Measurements on five axis machine tools,” CIRP, Vol.53, No.1, pp. 429-432, 2004.

**Membership in Academic Societies:**

- American Society of Precision Engineering (ASPE)
  - European Society for Precision Engineering and Nanotechnology (euspen)
- 



**Name:**  
Konrad Wegener

**Affiliation:**  
Professor, Institute for Machine Tools and Man-  
ufacturing (IWF), ETH Zürich

**Address:**  
Tannenstrasse 3, 8092 Zürich, Switzerland

**Brief Biographical History:**

1991 Ph.D., TU Braunschweig  
1999- Head of Design and Layout Planning Departments, Schuler Presses GmbH & Co. KG, Göppingen  
2003- CEO Schuler Held Lasertechnik, Heusenstamm  
2003- Head of Institute for Machine Tools and Manufacturing (IWF), ETH Zürich  
2011- CEO inspire AG for Mechatronic Production Systems and Manufacturing, Zürich

**Main Works:**

- “Conditioning and Monitoring of Grinding Wheels,” CIRP, Vol.60, No.2, pp. 757-777, 2011.
- “Phenomenological Compensation of Thermally caused Position and Orientation Errors of Rotary Axes,” J. of Manufacturing Processes, Vol.15, No.4, pp. 452-459, 2013.
- “Optimal control for chatter mitigation in milling, Part 1: Modelling and control design,” Control engineering practice, Vol.24, pp. 155-166, 2014.
- “Optimal control for chatter mitigation in milling, Part 2: Experimental validation,” Control engineering practice, Vol.24, pp. 167-175, 2014.
- “Open Loop Inertial Cross-talk Compensation Based on Measurement Data,” 25th Annual Meeting of The American Society for Precision Engineering, Atlanta, USA, 2010.

**Membership in Academic Societies:**

- The International Academy for Production Engineering (CIRP), Associate Member
-